Wave function matching in scattering matrix calculations for hard-wall nanostructures

1995 J. Phys.: Condens. Matter 7 745

(http://iopscience.iop.org/0953-8984/7/4/005)

J. Phys.: Condens. Matter 7 (1995) 745–758. Printed in the UK

Wave function matching in scattering matrix calculations for hard-wall nanostructures

P N Butcher† and J A McInnes‡

† Department of Physics, University of Warwick, Coventry CV4 7AL, UK

‡ Department of Computer Science, University of Strathclyde, Glasgow G1 1XH, UK

Received 21 June 1994, in final form 15 November 1994

Abstract. A nanostructure with hard walls is divided into two regions: the terminals and the 'cavity' that connects them. In the absence of a magnetic field the modes in the terminals may be written down immediately. The modes in the cavity are calculated by extending each terminal mode continuously into the cavity and applying hard-wall boundary conditions elsewhere on the cavity boundary. Then a general wave function ψ continuous everywhere may be written down. The relationships between the coefficients of the modes in ψ are determined by minimizing the mean square discontinuity in the normal derivative of ψ averaged over all the interfaces between the terminals and the cavity. This method has been found to be robust and efficient in calculations of the conductance matrix and scattering wave functions for a 2D quantum wire with a hard-wall finger of various shapes pushed in through one side.

1. Introduction

In the last decade the behaviour of two-dimensional (2D) electron gases in semiconductor nanostructures has been the subject of intense experimental and theoretical investigation [1–3]. In the theoretical studies it is usually supposed that the nanostructure has hard potential walls at which the electron wave function vanishes. Scattering matrices for such a system have been calculated either by considering the one-electron Green function [4–9] or by working directly with the electron wave function [7–18]. The Green function approach has wide generality and is well established. It yields scattering matrices relatively easily but not wave functions. The wave function approach easily yields both scattering matrices and wave functions. However, its use is usually restricted to nanostructures that can be broken into a number of regions in which the boundary geometry is simple enough to allow a complete set of wave functions to be written down. These functions are then superposed and their coefficients are related by matching the wave function and its normal derivative across all the interfaces between the regions. In this paper we consider the wave function approach from a different point of view, which allows a general formalism to be established. We test the usefulness of the new approach by applying it to a particular system that is fairly well understood [7–18].

Generality is achieved by recognizing that, in any nanostructure, there are only two *essentially* distinct regions. First we have the terminals through which electrons are injected or removed. Each terminal is modelled by a quantum wire with two parallel hard walls. Consequently we may immediately write down a complete set of modes in the terminals. In addition there is a central region that connects the terminals and is separated from them by interfaces we may choose at will. We call this region the 'cavity'. It often has a complicated geometry that makes it necessary to determine the cavity modes numerically. In doing so

0953-8984/95/040745+14$19.50

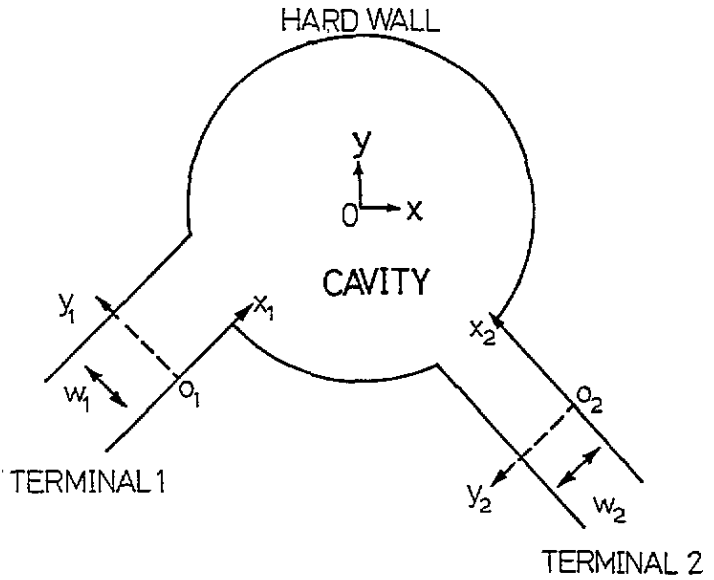

Figure 1. A schematic diagram of a hard-wall nanostructure.

we choose the boundary conditions in a way that makes it possible to *write down* a general cavity function that *automatically* matches the wave function in *every* terminal. Then we have only to match the normal derivative of the wave functions on either side of all the interfaces to obtain the equations that relate the coefficients of all the other modes to the coefficients of the incident terminal modes, which we suppose to be given.

The plan of the paper is as follows. In section 2 we establish an appropriate notation and carry through the formal programme outlined above. Section 3 is concerned with the numerical implementation of the formalism. In section 4 we describe the results obtained in the first application of this generalized matching procedure. The particular system considered is a 2D quantum wire with a finger of various shapes pushed in through one side. In section 5 we draw some conclusions and discuss the extension of the generalized matching method both to other structures and to allow for the presence of an applied magnetic field. In the present paper we set the magnetic field equal to zero.

2. General formalism

We consider a 2D nanostructure with N terminals. Figure 1 is a schematic diagram for $N = 2$. Oxy is a 'universal' coordinate system that can be chosen at will. The continuous line is the hard-wall boundary on which the wave function $\psi(x, y) = 0$. Within the nanostructure $\psi(x, y)$ is the solution of the Schrödinger equation for a free electron:

$$\partial^2\psi/\partial x^2 + \partial^2\psi/\partial y^2 + (2\pi/\lambda)^2\psi = 0. \tag{1}$$

Here λ is the de Broglie wavelength, which is related to the electron energy ϵ by

$$\epsilon = (\hbar^2/2m^*)(2\pi/\lambda)^2 \tag{2}$$

where m^* denotes the effective mass.

The parallel lines in figure 1 bound the terminals, which we label with a positive integer t. We also introduce an interface in terminal t, which we refer to as interface t (the dashed straight lines in figure 1) and a local coordinate system $O_t x_t y_t$ located and oriented as indicated. To be precise we define terminal t to be the region where $x_t < 0$. The cavity is the interior of the nanostructure, which is separated from the terminals by the interfaces.

Let w_t be the width of terminal t. A general solution of equation (1) in terminal t is

$$\psi(x_t, y_t) = \sum_m v_{tm}^{-1/2}[a_{tm}\exp(ik_{tm}x_t) + b_{tm}\exp(-ik_{tm}x_t)]u_{tm}(y_t). \tag{3}$$

Here m is a positive integer labelling the normalized mode functions

$$u_{tm}(y_t) = (2/w_t)^{1/2}\sin(m\pi y_t/w_t) \tag{4}$$

$$k_{tm} = [(2\pi/\lambda)^2 - (m\pi/w_t)^2]^{1/2} \tag{5a}$$

is the longitudinal wave number and

$$v_{tm} = \hbar|k_{tm}|/m^*. \tag{5b}$$

For propagating modes with $2w_t/\lambda > m$ we define k_{tm} to be positive. Then v_{tm} in equation (5*b*) is the magnitude of the electron velocity. Consequently a_{tm} (b_{tm}) in equation (3) is the coefficient of a 'forward' ('backward') wave that carries one electron per second into (out of) the nanostructure via terminal t. The factor $v_{tm}^{-1/2}$ is inserted into the right-hand side of equation (3) to achieve this convenient normalization. It has the consequence that the scattering matrix relating $\{b_{tm}\}$ to $\{a_{tm}\}$ for propagating modes is unitary.

For evanescent modes with $2w_t/\lambda < m$ we write $k_{tm} = i\kappa_{tm}$ where $\kappa_{tm} > 0$. Then a_{tm} is the coefficient of a 'forward' evanescent wave, which increases in magnitude away from the cavity. Consequently a_{tm} must be set equal to zero for all forward evanescent waves. On the other hand, b_{tm} is the coefficient of a 'backward' evanescent wave, which decays away from the cavity and is not restricted.

We set $x_t = 0$ in $\psi(x_t, y_t)$ and $\partial\psi(x_t, y_t)/\partial x_t$ in order to write down expressions for a general wave function and its normal derivative on interface t:

$$\psi(0, y_t) = \sum_m v_{tm}^{-1/2}[a_{tm} + b_{tm}]u_{tm}(y_t) \tag{6a}$$

$$\frac{\partial\psi(0, y_t)}{\partial x_t} = \sum_m v_{tm}^{-1/2} ik_{tm}[a_{tm} - b_{tm}]u_{tm}(y_t). \tag{6b}$$

We now seek a solution of Schrödinger's equation inside the cavity that reproduces $\psi(0, y_t)$ and $\partial\psi(0, y_t)/\partial x_t$ on every interface. It is convenient to approach this matching problem by using the universal coordinate system inside the cavity and expressing $\psi(x, y)$ there in terms of a carefully chosen set of cavity modes $\{\theta_{sm}(x, y)\}$ where s and m are both positive integers. The wave function $\theta_{sm}(x, y)$ satisfies Schrödinger's equation inside the cavity and the boundary conditions $\theta_{sm}(x, y) = u_{sm}(y_s)$ on interface s and $\theta_{sm}(x, y) = 0$ elsewhere on the cavity boundary and on all other interfaces. Consequently we can write the general wave function inside the cavity in the form

$$\psi(x, y) = \sum_s \sum_m v_{sm}^{-1/2}[a_{sm} + b_{sm}]\theta_{sm}(x, y) \tag{7a}$$

where the coefficient of $\theta_{sm}(x, y)$ has been chosen to make $\psi(x, y)$ in the cavity continuous with $\psi(x_t, y_t)$ in terminal t for all t. To check that continuity has been achieved we note that the above definition of $\theta_{sm}(x, y)$ implies that, as we approach interface t from inside the cavity, the cavity modes with $s = t$ are the only ones that contribute to $\psi(x, y)$ in equation (7*a*) and they reduce to $u_{tm}(y_t)$ on the interface. Consequently, $\psi(x, y)$ in equation (7*a*) reduces to $\psi(0, y_t)$ in equation (6*a*) on interface t for all t.

It remains for us to optimize the discontinuity of the normal derivative across all the interfaces. To consider the discontinuity at terminal t it is now convenient to regard $\psi(x, y)$ and $\theta_{sm}(x, y)$ as functions of the local coordinates (x_t, y_t). We write these functions in the simple forms $\psi(x_t, y_t)$ and $\theta_{sm}(x_t, y_t)$ respectively since no confusion with $\psi(x, y)$ and $\theta_{sm}(x, y)$ is likely to arise. Then, by differentiating equation (7*a*) with respect to x_t we find that

$$\frac{\partial \psi(x_t, y_t)}{\partial x_t} \to \sum_s \sum_m v_{sm}^{-1/2}[a_{sm} + b_{sm}]\frac{\partial \theta_{sm}(0, y_t)}{\partial x_t} \tag{7b}$$

as the point $(0, y_t)$ on the interface is approached from inside the cavity. When the same point is approached from inside the terminal the normal derivative is given by equation (6*b*). It is convenient to write that equation in the form

$$\frac{\partial \psi(0, y_t)}{\partial x_t} = \sum_s \sum_m v_{sm}^{-1/2} \mathrm{i} k_{sm}[a_{sm} - b_{sm}]\theta_{sm}(0, y_t). \tag{7c}$$

The right-hand sides of equations (6*b*) and (7*c*) are identical because $\theta_{sm}(0, y_t)$ vanishes when $s \neq t$ and is equal to $u_{tm}(y_t)$ when $s = t$. By subtracting the right-hand sides of equations (7*b*) and (7*c*) we obtain the following expression for the discontinuity of $\partial \psi(x_t, y_t)/\partial x_t$ at the point $(0, y_t)$ on interface t:

$$E_t(y_t) = \sum_s \sum_m [a_{sm}\phi_{smf}(y_t) + b_{sm}\phi_{smb}(y_t)]. \tag{8}$$

Here

$$\phi_{smf}(y_t) = v_{sm}^{-1/2}[\partial \theta_{sm}/\partial x_t - \mathrm{i} k_{sm}\theta_{sm}] \tag{9a}$$

and

$$\phi_{smb}(y_t) = v_{sm}^{-1/2}[\partial \theta_{sm}/\partial x_t + \mathrm{i} k_{sm}\theta_{sm}] \tag{9b}$$

where we leave it understood that θ_{sm} and $\partial \theta_{sm}/\partial x_t$ are to be evaluated at the point $(0, y_t)$ in the local coordinate system $O_t x_t y_t$. The subscripts f and b indicate that the functions so labelled are associated with forward and backward waves respectively.

In a scattering problem the coefficients $\{a_{sm}\}$ of all the forward waves are given. Then we may determine the real and imaginary parts of the coefficients $\{b_{sm}\}$ of all the backward waves so as to minimize the error function

$$E = \sum_t \int_0^{w_t} |E_t(y_t)|^2 \, \mathrm{d}y_t = \sum_t \int_0^{w_t} \mathrm{d}y_t \left| \sum_s \sum_m [a_{sm}\phi_{smf}(y_t) + b_{sm}\phi_{smb}(y_t)] \right|^2. \tag{10}$$

Thus we find the desired equations:

$$\sum_s \sum_m M^{\mathrm{bb}}_{s'm',sm} b_{sm} = -\sum_s \sum_m M^{\mathrm{bf}}_{s'm',sm} a_{sm} \tag{11}$$

where

$$M^{\mathrm{bb}}_{s'm',sm} = \sum_t \int_0^{w_t} \mathrm{d}y_t \, \phi^*_{s'm'\mathrm{b}}(y_t)\phi_{sm\mathrm{b}}(y_t) \tag{12a}$$

and

$$M^{\mathrm{bf}}_{s'm',sm} = \sum_t \int_0^{w_t} \mathrm{d}y_t \, \phi^*_{s'm'\mathrm{b}}(y_t)\phi_{sm\mathrm{f}}(y_t). \tag{12b}$$

To carry out calculations in a particular structure we keep enough terminal modes to secure convergence, calculate the integrals in equation (12) and solve a truncated set of equations (11) to express the coefficients $\{b_{sm}\}$ of the retained backward waves in terms of the coefficients $\{a_{sm}\}$ of the forward propagating waves. (We set $a_{sm} = 0$ for all evanescent modes.) The calculation yields b_{sm} for both propagating and evanescent modes. To calculate the element $S_{sm,tn}$ of the scattering matrix we set $a_{t'n'} = \delta_{tt'}\delta_{nn'}$ and calculate $b_{sm} \equiv S_{sm,tn}$ for all propagating modes in terminal s. Finally, the off-diagonal elements of the conductance matrix are given by

$$G_{st} = (2e^2/h)g_{st} \tag{13a}$$

when $s \neq t$. The factor of two allows for spin degeneracy and the normalized conductance g_{st} is given by

$$g_{st} = \sum_m \sum_n |S_{sm,tn}|^2. \tag{13b}$$

We note that G_{st} is the conductance between reservoirs as defined by Buttiker [19], which is the quantity usually measured in nanostructures. The conductance between leads originally discussed by Landauer [20] is not used here.

The wave function established by a specified combination of propagating forward waves is calculated by keeping b_{sm} for the evanescent modes and substituting both $\{a_{sm}\}$ and $\{b_{sm}\}$ into equations (3) and (7*a*). We discuss the matching procedure in more detail in appendix A.

3. Numerical implementation

We consider a 2D physical domain mapped onto a computational domain defined over a rectangular mesh of maximum size 480 × 480. Meshes up to this size have been found to be appropriate for all profile shapes and physical domains investigated. For more regular structures smaller mesh sizes are adequate; indeed sensible results may be obtained for meshes as small as 120 × 120.

The profile of the intrusions into the cavity is defined analytically and superimposed onto the mesh. The value of the wave function ψ on the boundary and around the intrusions is set equal to zero, with appropriate non-zero values on the boundary of each terminal in turn. An advantage of our computational procedure is that both the physical domain and the intrusion profile may be of arbitrary shape, thus allowing wave function matching to be performed in nanostructures of any shape.

The evaluation of ψ at all interior points is achieved by solving the discretized Schrödinger equation directly. Schrödinger's equation is approximated by a set of sparse linear equations which, after LU decomposition, is solved for ψ. The values of ψ thus

computed correspond to a particular mode in a specific terminal, i.e. a terminal–mode pair. The above procedure is repeated for several modes in all terminals, creating a set of ψ values on each occasion. As is clear from the formalism there is, for a particular de Broglie wavenumber, a finite number of propagating modes and an infinite number of evanescent nodes. Investigations into the number of evanescent modes to be included in the computations have shown that, for structures sufficiently far away from the terminals, there is no significant advantage achieved by including more than five evanescent modes. Consequently all computations include five evanescent modes and the appropriate number of propagating modes.

For each set of ψ values the derivatives across the appropriate interface are computed numerically. Once the values of ψ and its derivative are known for all terminal–mode pairs it is straightforward to solve the set of complex linear equations relating the derivatives and the coefficients $\{b_m\}$. From the resulting $\{b_m\}$ the scattering matrix for a specific terminal–mode pair is easily calculated, and hence the conductance g_{12} follows. Thus we may plot the variation of g_{12} with $2w/\lambda$ where w is the width of the channel and λ is the de Broglie wavelength. In order to plot the wave function contours we select an input propagating mode in a particular terminal and use the corresponding ψ values computed for all modes in all terminals to obtain $|\psi|^2$ for the terminal–mode pair. It is a trivial extension to obtain wave function contours once the scattering matrix has been computed.

All computations have been performed on the Cray Y-MP/8 at the Rutherford Appleton Laboratory with the graphical postprocessing on a Sun SparcStation. The code has been optimized to take advantage of the multiprocessor Y-MP/8 architecture and permits efficient automated generation of conductances and wave functions for arbitrarily shaped intrusions into arbitrarily shaped 2D structures over a range of wave vectors. Subsequent papers will show the application of the method to resonant ballistic structures and to disordered structures. The introduction of a magnetic field into the computational algorithm is straightforward and is currently under development.

4. Applications of the formalism

As a preliminary indication of the power of the formalism developed in sections 2 and 3 we present results obtained by applying it to three simple structures. The first structure is shown in figure 2. It consists of a 2D quantum wire with width w into which is introduced a flat-topped finger with height h and width d. The width $w' = w - h$ of the aperture above the finger plays a dominant role in determining the behaviour of this structure [7]. The cavity lies between the dashed lines and has length $L = 2w$ in all our calculations. The second structure is obtained by capping a flat-topped finger with a hard-wall semicircle of radius $d/2$ (shown dotted in figure 2). In this case w' denotes the open aperture above the top of the semicircle and h is the total height of the capped finger. In the third structure, which we consider only briefly, the finger has a Gaussian shape we describe later on.

The curves in figure 3 show the dependence of the normalized conductance g_{12} on $2w/\lambda$ calculated for the first structure when $d = 0.4w$ and $w' = w$ (i.e. for an open quantum wire), $0.3w$ and $0.1w$. The open quantum wire is cut off when $2w/\lambda < 1$ and N modes propagate through it when $2w/\lambda > N$. We see that the calculated values of g_{12} have the familiar staircase structure [1–3] in which g_{12} increases by one each time a new mode propagates in the quantum wire. For $w' = 0.3w$ and $0.1w$ the behaviour of g_{12} has a similar structure, as expected, but it is now the number of modes M propagating above the finger that determines the height of the plateaus. Steps occur when $2w'/\lambda$ is equal to M, i.e. when $2w/\lambda = Mw/w' = 3.33M$ and $10M$ when $w'/2 = 0.3$ and 0.1 respectively.

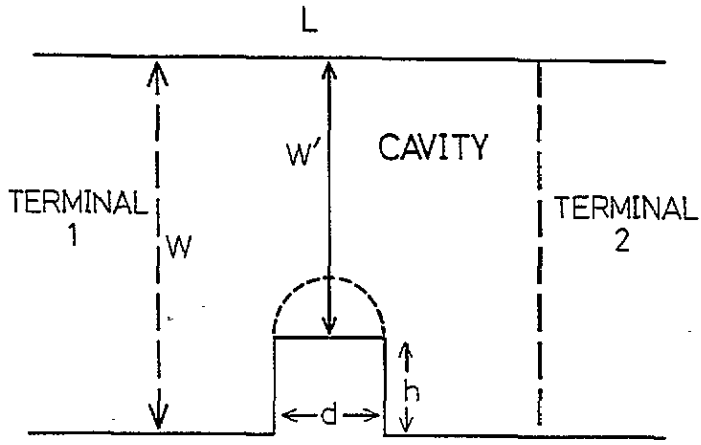

Figure 2. The nanostructure considered in the calculations. The dotted curve is a semicircular, hard-wall cap.

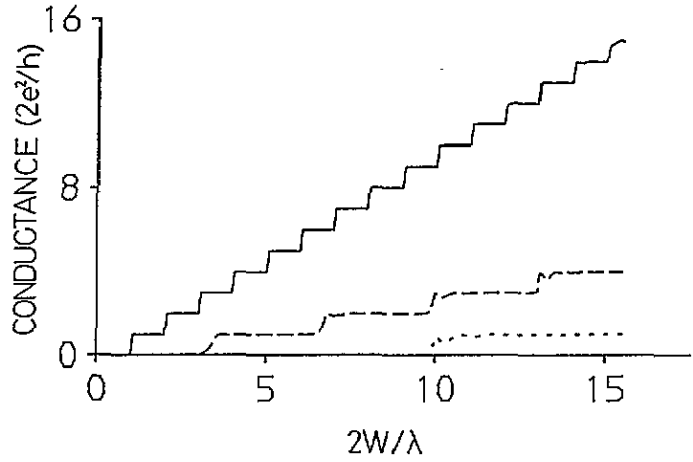

Figure 3. The dependence of the normalized conductance g_{12} on $2w/\lambda$, where λ is the de Broglie wavelength, for a flat-topped finger when $d = 0.4w$ and $w' = w$ (full line), $0.3w$ (dashed line) and $0.1w$ (dotted line).

The quantization of g_{12} when $w' = w$ is a trivial consequence of the diagonal scattering matrix for this case: $|S_{1m,2n}|^2 = \delta_{mn}$. We therefore see immediately from equations (13) that $g_{12} = N$. The quantization of g_{12} when $w' < w$ is more subtle. It is interesting, in this regard, to look more closely at the contributions to g_{12} for the point $2w/\lambda = 5$ on the dashed curve in figure 3 ($w' = 0.3w$). This point is on the first plateau and we chose it because it lies beyond the initial oscillations of g_{12} on the plateau, which are discussed below. There are four propagating modes in the quantum wire and one in the region above the finger if we regard that as a narrow quantum wire. We see from equations (13) that this is the sum of the calculated values of $|S_{1m,2n}|^2$, which are given in table 1.

We see that the entries in the table are nearly symmetrical. The exact entries would be completely symmetrical because the structure we consider is symmetrical. We have taken no

Table 1. Contributions to g_{12}.

m	$n=1$	$n=2$	$n=3$	$n=4$
1	0.036 32	0.078 10	0.058 68	0.018 50
2	0.075 98	0.164 80	0.125 70	0.040 17
3	0.055 77	0.122 60	0.095 25	0.030 81
4	0.017 78	0.039 39	0.030 81	0.009 751

steps to incorporate this fact into the calculation. Consequently the deviations of the entries in the table from a symmetrized version of it provide a measure of our numerical error. In the worst case ($m = 3$, $n = 1$) the error is 2.5%. This could be improved by decreasing the mesh size or increasing the number of evanescent modes. However, doing either of these things has a negligible effect on the quantities of direct interest to us: g_{12} and the wave function contours. The exact sum of all the entries in the table is $g_{12} = 1.00041$, which is unity to a much greater accuracy than we would expect. We quote this figure because it is representative of a general feature of our results: when quantization occurs it is achieved with much higher accuracy than would be expected from the accuracy of $|S_{1m,2n}|^2$. With or without symmetrization, there are no special features of the array in table 1 that help one to understand why the sum of the entries in it add up to a number close to one. They do so because the quantization reflects the internal geometry of the cavity [7] as discussed in appendix B.

We see in figure 3 small oscillations of g_{12} at the beginning of each plateau when $w' \neq w$. They are due to interference between the waves reflected by the sharp corners on the top of the finger [7, 8]. If this interpretation is correct we would expect the oscillations to disappear if the finger were capped with a hard-wall semicircle as shown by the dotted curve in figure 2. We test this expectation by using the calculated results presented in figure 4. The full line reproduces the plot already given for a flat-topped finger with $d = 0.4w$ and $w' = 0.3w$. It is to be compared with the dashed line, which shows the behaviour of g_{12} when the same aperture is achieved by using a flat-topped finger of the same width but with height $0.5w$ and capping it with a semicircle of radius $0.2w$. We see that the plateaus remain well developed and are indeed free from interference oscillations. Rounding off the top of the finger also broadens the rising edges between plateaus.

The dotted curve in figure 4 shows the behaviour of g_{12} for a finger with a Gaussian shape. The height at a distance x away from the centre of the finger is given by $H(x) = h\exp(-x^2/2\sigma^2)$ where $\sigma = 0.3w$ so that $H(x)$ is small on the interfaces. We put $h = 0.7w$ so that the maximum finger height and the aperture above it are the same as for the other two curves in figure 4. Nevertheless, we see that the behaviour of g_{12} is different. It keeps the same step size, achieves integer values near the centres of what are good plateaus on the other two curves and shows no oscillations but flat plateaus are not formed. This is because the radius of curvature at the top of the Gaussian finger is only 0.28 of that of the capped finger. The region above the finger is consequently too narrow for good plateaus to form. The behaviour of the thin finger with $w' = 0.3w$ shown in figure 5 is similar.

The curves in figure 5 are calculated for thin, flat topped fingers with $d = 0.0667w$. The strict staircase (full curve) is the open quantum wire result for $w' = w$. When w' is reduced to $0.8w$ (dashed curve) the very tiny finger is beginning to have effects on the step length, plateaus and rising edges but the effects are much less than they are for broad fingers. When $w' = 0.5w$ (dotted curve) the step length has increased to two, as it does for broad fingers, but there are no plateaus. We find cusps at the expected values of $2w/\lambda = 2, 4, 6, 8, \ldots$ and

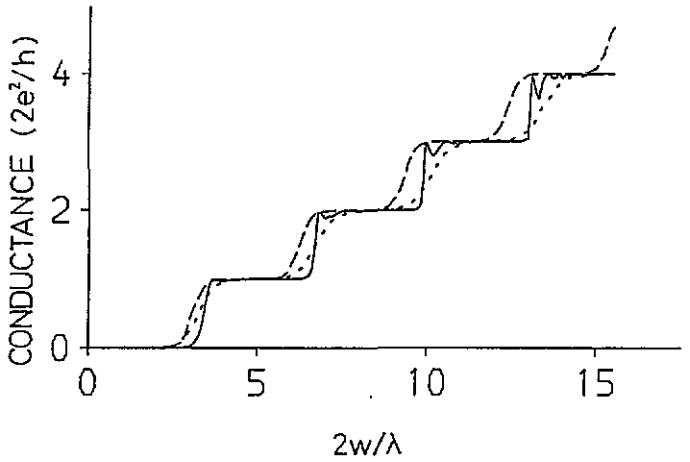

Figure 4. The dependence of the normalized conductance g_{12} on $2w/\lambda$ where λ is the de Broglie wavelength. The full curve is for a flat-topped finger that leaves open an aperture $w' = 0.3w$. The dashed line is for a finger capped by a semicircle that leaves open the same aperture. In both cases the width of the finger is $d = 0.4w$. The dotted curve shows the behaviour for the Gaussian shaped finger described in the text, which also has $w' = 0.3w$.

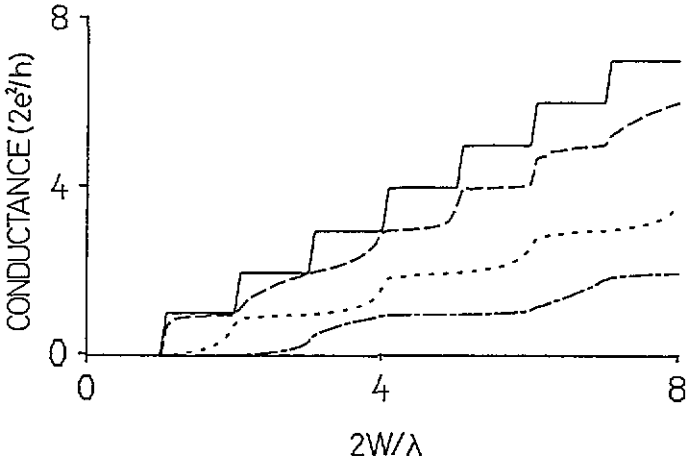

Figure 5. The dependence of the normalized conductance g_{12} on $2w/\lambda$, where λ is the de Broglie wavelength, for thin fingers with flat tops. The thickness $d = 0.0667w$ in all cases and $w' = w$ (full line), $0.8w$ (dashed line), $0.5w$ (dotted line) and $0.3w$ (dashed–dotted line).

continuously rising curves between these points which never quite rise to the next integer value of g_{12} before the next cusp occurs. Finally, when $w' = 0.3w$, (dot–dashed curve) we find weakly formed plateaus with continuously rising curves between them.

In figures 6, 7 and 8 we show contour plots for $|\psi|^2$ inside the cavity. In every case the incident wave is mode 1 in terminal 1, i.e. the only non-vanishing coefficient a_{tm} in equation (3) is a_{11}, which is set equal to unity. The contour plots are therefore concentrated on the left of the finger in all three figures. The plots are all for the same structure, which has a centrally placed, flat-topped finger with width $0.3w$ and height $0.7w$. Figure 6 is for

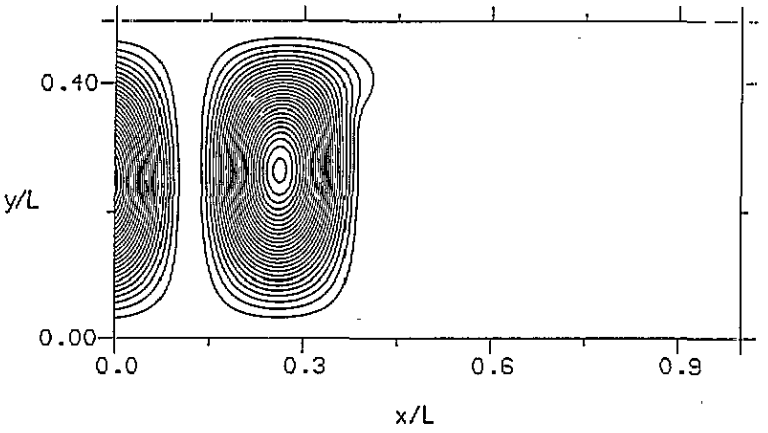

Figure 6. Wave function contours when $d = 0.4w$, $w' = 0.3w$ and $2w/\lambda = 2$ (no transmission).

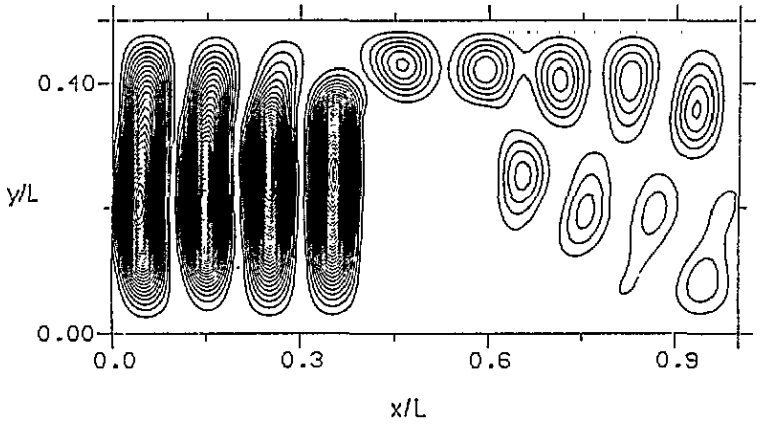

Figure 7. Wave function contours when $d = 0.4$, $w' = 6.3w$ and $2w/\lambda = 5$ (first plateau).

$2w/\lambda = 2$ where λ is the de Broglie wavelength. We see from the dashed curve in figure 3 that there is negligible propagation over the finger in this case. Consequently, the contours extend only a small distance into the region over the top of the finger. The longitudinal period of the strong standing wave pattern on the left of the finger is equal to half the longitudinal wavelength of the dominant ($n = 1$) mode there. Moreover, we note that one half wavelength is fitted in between the walls of the terminals. Thus, the behaviour of the standing wave pattern on the left is controlled by the incident wave, which is the only propagating mode there when $2w/\lambda = 2$.

Figure 7 is for $2w/\lambda = 5$, which is in the middle of the first plateau in figure 3. Thus, one mode can now propagate over the finger and this mode consequently determines the standing wave pattern there. On the left the standing wave pattern is again determined by the incident wave. On the right of the finger four waves can propagate and a complicated standing wave pattern develops from their interference.

Finally, figure 8 is for $2w/\lambda = 8$, which is on the second plateau in figure 3. The incident wave again determines the standing wave pattern on the left. Over the finger the dimensions of the structure of $|\psi|^2$ are commensurate with the $n = 2$ mode dominating

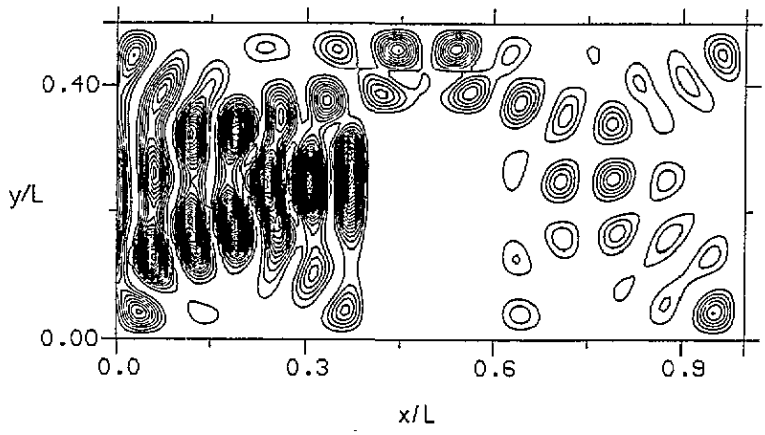

Figure 8. Wave function contours when $d = 0.4w$, $w' = 0.3w$ and $2w/\lambda = 8$ (second plateau).

there while, on the right, seven modes can propagate and the standing wave pattern again shows considerable structure as a result of their interference.

5. Conclusion

The matching procedure described in this paper can be used to calculate wave functions, scattering matrices and conductance matrices for nanostructures with many different geometries. In the structures considered here the new matching procedure has been found to be fast, accurate and robust. Some of the structures studied can also be investigated by using conventional matching [7]. To do that it is necessary to insert more interfaces into the cavity so that the wave function in each region can be expressed as the sum of a series of analytic functions. Then both the wave function and its normal derivative are matched across every interface. We have included two cases in which this approach fails: firstly, when the finger is capped with a semicircle, and secondly, when it has a Gaussian profile. Neither of these finger profiles yields a set of analytic functions. In our new procedure the required set of cavity functions is generated numerically. Consequently, arbitrary cavity geometries can be treated almost as fast as simple ones. In another paper we discuss the resonant tunnelling that occurs when two identical fingers are pushed into the cavity [21].

We have concentrated on ballistic transport. However, the introduction of random scattering centres into the cavity is easily accomplished. The required potential has only to be specified prior to the determination of the cavity wave functions [22]. The calculation becomes particularly simple when a white noise potential is set up on the numerical mesh used to calculate the cavity functions [3, 8, 13]. Finally, the formalism is easily modified to allow for the presence of a constant magnetic field throughout the nanostructure [18]. In this case, however the terminal modes must be calculated numerically in addition to the cavity functions. This additional calculation has a 1D character and does not significantly affect the running time of the programme [17, 23]. Finally, the formalism used here for 2D electron gases is easily generalized to handle 3D structures. The computing time, however, will escalate considerably when 3D structures are considered.

Acknowledgments

The authors are grateful to the SERC for financial support. They would also like to thank the referees for their constructive criticisms of the original manuscript.

Appendix A. Comments on the matching procedure

We show, first of all, that any exact solution $\psi(x, y)$ of the scattering problem has coefficients $\{a_{tm}\}$ and $\{b_{tm}\}$ that satisfy the matching equations (11) and give $E = 0$ in equation (10). Thus, given $\psi(x, y)$, we may immediately determine $\{a_{tm}\}$ and $\{b_{tm}\}$ from equations (6) because the mode functions $\{u_{tm}(y_t)\}$ are orthonormal. Inside the cavity we know that $\psi(x, y)$ has the following properties: it satisfies the wave equation (1), it is equal to (6*a*) on each interface t and it vanishes elsewhere on the cavity boundary. These conditions determine $\psi(x, y)$ uniquely inside the cavity. The cavity functions $\{\theta_{sm}(x, y)\}$ have been specifically defined to ensure that the right-hand side of equation (7*a*) has precisely these properties. It is consequently a correct representation of $\psi(x, y)$ inside the cavity. The discussion in section 2 therefore yields equation (8) for the discontinuity of the normal derivative $E_t(y_t)$ across interface t, which vanishes because $\psi(x, y)$ is an exact solution of the scattering problem. Consequently the error function E in equation (10) also vanishes. Moreover, when we set $E_t(y_t) = 0$ in equation (8), multiply by $\phi^x_{s'm'b}(y_t)$, integrate over the interface and sum over t the result is equation (11), on which all our subsequent calculations are based. Thus as stated, $E = 0$ and equation (11) is satisfied for an exact scattering wave function.

When we seek an approximate solution of equation (11) we keep only a finite number N of the modes in the terminals together with their associated cavity functions. We also keep only the N equations (11) that involve these functions in the coefficients $M^{bb}_{s'm',sm}$ and $M^{bf}_{s'm',sm}$. Then the equations have a unique solution. The error function is no longer zero but the equations (11) ensure that it has the minimum value that can be achieved in the truncated function space.

Finally, we note that the sum over t in equation (10) plays no role when we consider an exact solution because $E_t(y_t) = 0$ for all t. However, it has an important function when we seek approximate solutions because it gives equal weight to the contribution to the error function from each interface.

Appendix B. Quantization in quantum wire structures

We sketch a flat-topped finger structure in figure 1 consisting of three quantum wires: terminal 1, terminal 2 and region 3, which is the space over the top of the finger. Provided region 3 is long enough, we may use a scattering matrix description of the entire structure as illustrated in figure B1. The rectangular boxes show schematically the connection of region 3 to terminal 1, which is described by a scattering matrix $\mathbf{S}$ and the connection of terminal 2 to region 3 which is described by another scattering matrix $\mathbf{Z}$. We write $\mathbf{a}_1$, $\mathbf{b}_3$ and $\mathbf{b}_2$ for the column matrices of the coefficients of waves travelling to the right in the regions indicated. Similarly we write $\mathbf{b}_1$, $\mathbf{a}_3$ and $\mathbf{a}_2$ for the column matrices of coefficients of waves travelling to the left.

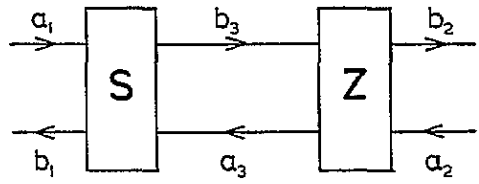

Figure B1. A schematic diagram of the scattering matrices at each end of a flat-topped finger and the associated incident and reflected waves.

We may express the relationships between these quantities in a partitioned form:

$$\begin{aligned} \mathbf{b}_1 &= S_{11}\mathbf{a}_1 + S_{13}\mathbf{a}_3 \\ \mathbf{b}_3 &= S_{31}\mathbf{a}_1 + S_{33}\mathbf{a}_3 \end{aligned} \tag{B1}$$

and

$$\begin{aligned} \mathbf{b}_2 &= Z_{22}\mathbf{a}_2 + Z_{23}\mathbf{b}_3 \\ \mathbf{a}_3 &= Z_{32}\mathbf{a}_2 + Z_{33}\mathbf{b}_3. \end{aligned} \tag{B2}$$

As Szafar and Stone have emphasized [7], quantization may be expected when waves incident from region 3 are not reflected, i.e. when $S_{33} = Z_{33} = 0$. Then we may immediately eliminate $\mathbf{a}_3$ and $\mathbf{b}_3$ from the above equations to find the scattering matrix connecting terminals 1 and 2:

$$\begin{aligned} \mathbf{b}_1 &= S_{11}\mathbf{a}_1 + S_{13}Z_{32}\mathbf{a}_2 \\ \mathbf{b}_2 &= Z_{23}S_{31}\mathbf{a}_1 + Z_{22}\mathbf{a}_2. \end{aligned} \tag{B3}$$

Moreover, in zero magnetic field, we know that both the rows and the columns of a scattering matrix form an orthonormal set of vectors. Since $S_{33} = Z_{33} = 0$ we see from equations (B1) and (B2) that

$$\sum_{i=1}^{N} S_{ik}^{13}(S_{i\ell}^{13})^* = \delta_{k\ell} \tag{B4}$$

and

$$\sum_{j=1}^{N} Z_{kj}^{32}(Z_{\ell j}^{32})^* = \delta_{k\ell} \tag{B5}$$

where both k and ℓ take integer values $1, 2, \ldots, M$. Here N is the number of modes propagating in terminals 1 and 2 and M is the number of modes propagating in region 3.

With these preliminaries we may immediately manipulate equation (13*b*) to show that $g_{12} = M$. Thus we have, in an obvious notation,

$$\begin{aligned} g_{12} &= \sum_i \sum_j (S_{13}Z_{32})_{ij}(S_{13}Z_{32})_{ij}^* = \sum_i \sum_j \sum_k \sum_\ell (S_{ik}^{13}Z_{kj}^{32})(S_{i\ell}^{13}Z_{\ell j}^{32})^* \\ &= \sum_i \sum_j \sum_k \sum_\ell (S_{ik}^{13}S_{i\ell}^{13*})(Z_{kj}^{32}S_{\ell j}^{32*}) = \sum_k \sum_\ell \delta_{k\ell}^2 = M. \end{aligned} \tag{B6}$$

Thus, while diagonality of the scattering matrix is sufficient for quantization, it is not necessary. For the structure shown in figure 1 we find that g_{12} is well quantized when there is strong channel mixing because there is negligible backscattering of waves leaving the region above the finger.

References

[1] Beenakker C W J and van Houten H 1991 *Solid State Physics* vol 44, ed H Ehrenreich and D Turnbull (San Diego: Academic) p 1

[2] Buttiker M 1990 *Semiconductors and Semimetals* vol 35, ed M A Reed (New York: Academic) pp 191–271

[3] Ulloa S E, MacKinnon A, Castano E and Kirczenow G 1992 *Handbook on Semiconductors* vol 1, ed P T Landsberg (Amsterdam: North-Holland) p 863

[4] Fisher D S and Lee P A 1981 *Phys. Rev.* B **23** 6851

[5] MacKinnon A 1985 *Z. Phys.* B **59** 385

[6] Stone A D and Szafar A 1988 *IBM J. Res. Dev.* **32** 384

[7] Szafar A and Stone A D 1990 *Phys. Rev. Lett.* **62** 300

[8] Baranger H U and Stone A D 1989 *Phys. Rev.* B **40** 8169

[9] Baranger H U, DiVicenzo D P, Jalabert R A and Stone A D *Phys. Rev.* B **44** 10637

[10] Kirczenow G 1988 *Solid State Commun.* **68** 715

[11] Kirczenow G 1989 *J. Phys.: Condens. Matter* **1** 305

[12] Kirczenow G 1989 *Phys. Rev.* B **39** 10452

[13] Maslov D L, Barnes C and Kirczenow G 1993 *Phys. Rev.* B 48 2543

[14] Escapa L and Garcia N 1989 *J. Phys.: Condens. Matter* **1** 2125

[15] Garcia N and Escapa L 1989 *Appl. Phys. Lett.* 54 1418

[16] Tekman E and Ciraci S 1989 *Phys. Rev.* B **39** 8772

[17] Avishai Y and Band Y B 1989 *Phys. Rev.* B 40 3429, 12535; *Phys. Rev. Lett.* **62** 2527; 1990 *Phys. Rev.* B **41** 3253; 1991 *Phys. Rev. Lett.* **66** 1761

[18] Ji Z-L and Berggren K-L 1992 *Phys. Rev.* B 45 6652

[19] Buttiker M 1986 *Phys. Rev. Lett.* **57** 1761; *IBM J. Res. Dev.* **32** 317

[20] Landauer R 1957 *IBM J. Res. Dev.* **1** 233; 1970 *Phil. Mag.* **21** 863

[21] Butcher P N and McInnes J A In preparation

[22] Nixon J A, Davies J H and Baranger H U 1991 *Phys. Rev.* B **41** 7929

[23] Schult R L, Ravenhall D G and Wyld H W 1990 *Phys. Rev.* B **41** 12760